1-2-2023

Wavelet-Based Harmonic Magnitude Measurement in the Presence of Interharmonics

Flavio Costa
Michigan Technological University, fbcosta@mtu.edu

Stefan Häselbarth
Technische Universitat Berlin

Sergey Yanchenko
Moscow Power Engineering Institute (Technical University)

Kai Strunz
Technische Universität Berlin

Aurenice M. Oliveira
Michigan Technological University, oliveira@mtu.edu

Wavelet-Based Harmonic Magnitude Measurement in the Presence of Interharmonics

Flavio B. Costa, Stefan Häselbarth, Sergey Yanchenko, Kai Strunz, Aurenice M. Oliveira,

Abstract—The increasing proliferation of power electronic converters, nonlinear loads, and distributed generation are leading to increased levels of harmonic and interharmonics in power networks. As a consequence, power quality (PQ) has become a critical performance indicator for power utilities and end-users. This study proposes a novel harmonic estimation method based on the real-time stationary discrete wavelet packet transform (RT-SDWPT). The proposed technique decomposes an input signal into frequency bands with harmonic information at cutoff frequencies and uses a compensation strategy to estimate root mean square (RMS) values of harmonics at every sampling period. The performance and effectiveness of the proposed method are assessed using real measurement data from field cases and experimental setup. The real measurements include challenging scenarios with harmonics, subharmonics, interharmonics, frequency deviation, and non-stationary PQ events. The proposed method outperforms the harmonic estimation provided by the discrete Fourier transform (DFT)-based approach and existing wavelet packet-based methods in terms of accuracy and speed.

Index Terms—Harmonic measurements, power quality indices, stationary discrete wavelet packet.

I. INTRODUCTION

In recent years, the substantial increase of harmonic and interharmonic distortion in power systems caused by the proliferation of power electronics converters, nonlinear loads, and distributed generation has generated power quality (PQ) concerns to power utilities and end-users alike. It is critical for power network operators to have an accurate knowledge of harmonics present in the system to assess power quality performance. Furthermore, the development of accurate harmonic phasor estimation algorithms is essential for the control, monitoring, and protection of smart grids [1]–[5]. Harmonic phasor measurement includes magnitude, phase, frequency, and rate of change of frequency (ROCOF). This paper focuses on the harmonic magnitude estimation.

The root mean square (RMS) value of fundamental and harmonic components of voltages and currents characterizes most PQ events, including non-stationary PQ and stationary PQ disturbances, such as voltage sags and harmonic distortions, respectively. Therefore, international standards have established ways for estimating and measuring harmonics and power based on RMS values of fundamental and harmonic components of voltages and currents. These standards include the International Electrotechnical Commission (IEC) Standard 61000-4-7 [6] and IEEE Standard 1459-2010 [7]. Most standards recommend the use of discrete Fourier Transforms (DFTs) for analyzing fundamental and harmonic components, which requires a periodic and stationary signal inside the RMS window. However, the RMS values of harmonics extracted by DFTs can present non-existing oscillations due to spectral leakage and picket fence effects when the signal contains non-synchronous frequency components, such as sub- and inter-harmonics, and non-stationary PQ disturbances. According to the IEC Standard 61000-4-7 [6], an RMS window with a time interval of 0.2 seconds can solve part of these drawbacks. However, long RMS windows yield significant time delays, limiting the DFT application for the real-time estimation of harmonic distortions.

Modified versions of the DFT have been used to minimize the main drawbacks of the DFT [8]–[11]. Methods based on cosine and mimic filters [12], [13] have demonstrated better performance than the DFT, especially for estimating the fundamental component in signals with decaying direct current (DC) offset [14]. Methods based on artificial intelligence [15]–[17], recursive last squares or least mean-square (LMS) [18], [19], Kalman filter [20]–[22], and other techniques [2], [23] have been used for harmonic estimation. However, none is affirmed to be effective in signals with interharmonics. Some methods have been proposed to estimate harmonics and interharmonics [24]–[26]. However, most of them do not consider challenging cases, such as near interharmonics on both sides of harmonics and with relevant magnitude.

The discrete wavelet transformation (DWT) overcomes some of the DFT limitations. Hence, it has been proposed for monitoring, detecting, and extracting PQ disturbances in power systems for quickly and effectively analyzing stationary and non-stationary signals [27]–[47]. DWT has been successfully applied for non-stationary signals such as the automatic diagnosis of faults, voltage sags, and switching operations [27]. Furthermore, the analysis of stationary PQ events has also been performed with the DWT [28]–[41]. Studies of power measurement using wavelet-based power and harmonic estimation methods have been previously investigated [42]–[47]. [42], [43] proposed DWT-based methods to estimate RMS values as well as active and reactive power. [44], [45] reformulated PQ indices defined in the IEEE Standard 1459-2010 using DWT. However, the DWT has a few limitations, including: 1) it presents non-uniform frequency bandwidth, resulting in problems for measuring harmonic components [37]; 2) it is a time-variant transformation. Thus, the coefficients are not computed in every sampling time due to the down-sampling process, resulting in inaccuracies under non-stationary PQ disturbances [29]. Moreover, DWT only decomposes the scaling coefficients from the first level, whereas the discrete wavelet packet transform (DWPT), a time-variant transformation, decomposes both scaling and wavelet coef-

ficients [38]. Therefore, the DWPT decomposition provides uniform output frequency bands, overcoming one of the DWT limitations. This is essential for identifying harmonics by selecting a suitable sampling frequency and wavelet-packet decomposition tree [37]–[39], [48]–[53]. Because DWPT is time variant, PQ estimation methods based on either the DWT or DWPT are usually not designed and embedded in hardware to provide the real-time progress of harmonic distortions [40], [41].

The stationary DWPT (SDWPT), on the other hand, presents both uniform frequency bandwidths and the time-invariant property, overcoming the limitations of both the DWT and DWPT. SDWPT is ideal for estimating PQ indices and detecting PQ disturbances as well as it is suitable to be embedded in hardware for the real-time PQ analysis by its real-time version (RT-SDWPT). [41] used the RT-SDWPT for the real-time estimation of odd harmonics.

Some DWPT- and SDWPT-based methods decompose input signals keeping the fundamental and odd harmonics centered on frequency bands and even harmonics located on cutoff frequencies [37], [41], [50]. The frequency bandwidths are twice the fundamental frequency ($2f$), referred in this paper as $2f$-band methods. Therefore, $2f$-band methods can be appropriately used for harmonic estimation when the original signal presents only odd harmonics. As an example, the study presented in [41] only provides accurate harmonic estimation when the power system presents neither even harmonics nor a DC component.

Other wavelet packet-based methods decompose input signals into output bandwidths of $f/2$ Hz, designated as $f/2$-band methods. After the decomposition, these bands are grouped in pairs to keep odd and even harmonics with unitary gain and centered on new frequency bands [48], [51], [52]. As an advantage, these methods estimate RMS values of both odd and even harmonics. However, these $f/2$-band methods evaluate output signals with a bandwidth of f Hz, which is two times higher than the original output signals due to the grouping of bands. The existing $f/2$-band methods are adversely affected by interharmonics. Then, most of the $f/2$-band methods use a long RMS window, as indicated in the IEC Standard 61000-4-7 [6], to reduce the effects of interharmonics. Nevertheless, this strategy does not work for all interharmonic frequencies and results in a significant time delay. Even using a one-cycle RMS window, these $f/2$-band methods introduce considerable time delay in the estimated RMS value during non-stationary PQ disturbances due to the number of decomposition levels and high-order mother wavelets.

This paper proposes a novel $f/2$-band method for the real-time magnitude estimation of harmonics, even in the presence of interharmonics. In contrast to the aforementioned existing $f/2$-band methods, the proposed method does not group the output frequency bands and uses the RT-SDWPT to benefit from uniform frequency bandwidths and time-invariant properties. The main advantages of the proposed methods are as follows: 1) the output signals have a narrow bandwidth of $f/2$ Hz and two output signals estimate harmonics redundantly. Consequently, harmonic measurements are less distorted by subharmonics and interharmonics; 2)

the proposed method can effectively detect transient events, changing the mother wavelet and the RMS window size during signal transitions to substantially reduce the time delay during non-stationary PQ disturbances. Consequently, the proposed method can adequately identify the time-variation of harmonic distortions; 3) the proposed method works well with a one-cycle RMS window and does not need a long window size as recommended by the IEC Standard 61000-4-7, avoiding long time delays and providing good results even in the presence of interharmonics with a frequency non-multiple of 5 Hz. Nevertheless, long window sizes are also possible for outstanding results if the time delay is not a problem.

The performance of the proposed method was compared to existing DFT, wavelet, and Kalman filter-based methods by considering actual data with stationary and non-stationary PQ disturbances. Some actual data were obtained in a laboratory with known harmonic, subharmonic, and interharmonic components. The performance evaluation considered the following events: subharmonics, multiple interharmonics, harmonic fluctuations, frequency deviation, non-stationary PQ disturbances, and time-varying harmonics, as well as the following facts: mother wavelet, sampling frequency, and RMS window size. The proposed method provided the best performance for estimating RMS values of harmonics.

II. REVIEW OF RMS VALUE REAL-TIME COMPUTATION

The RMS value of the hth harmonic component of a discrete-time domain signal x is a function of the related spectral energy $\mathcal{E}^h$ as follows:

$$X_{\mathrm{RMS}}^h(k) = \sqrt{\frac{\sum_{n=k-N+1}^{k}[x^h(n)]^2}{N}} = \sqrt{\frac{\mathcal{E}^h(k)}{N}}, \quad (1)$$

where $h=\{1,2,3,...,h_{max}\}$ is the harmonic order. For the sake of notational simplicity, the fundamental component at the frequency f=50 or 60 Hz is referred to as the first harmonic with h=1; $h_{max} = \lfloor f_s/(2f) \rfloor$ is the highest possible harmonic component of x, where f_s is the sampling frequency; the spectral energy of the hth harmonic component $\mathcal{E}^h$ is designated as the hth harmonic energy, which is obtained by the proposed wavelet-based method and presented in Section IV. N is the window size used to compute the RMS value, referred to as RMS window size; and k is the current time index associated with the current discrete time k/f_s. Since the proposed method is designed to run in real-time, samples associated with $k+n$, with $n=\{1,2,3,...\}$, are not used.

III. REVIEW OF THE REAL-TIME SDWPT

Based on [54], the RT-SDWPT decomposition packet coefficients with a frequency bandwidth of Δf are obtained, in real-time, by convolving the input signal with a pair of low- and high-pass finite impulse response (FIR) quadrature mirror filters (h_φ and h_ψ), as follows [55]:

$$s_{\Delta f}^{2z}(k) = \frac{1}{\sqrt{2}} \sum_{l=0}^{L-1} h_\varphi(l) s_{2\Delta f}^z(k+l-L+1), \quad (2)$$

$$s_{\Delta f}^{2z+1}(k) = \frac{1}{\sqrt{2}} \sum_{l=0}^{L-1} h_\psi(l) s_{2\Delta f}^z(k+l-L+1), \quad (3)$$

where $0 \leq z < Z_j$ is the packet node, $Z_j = 2^{j-1} - 1$ the highest node at the scale j; Δf is the frequency bandwidth of the packet coefficients at the scale j; $s_{f_s/2}^0$ is the original signal ($s_{f_s/2}^0 = x$); L is the length of the filters h_φ and h_ψ.

The packet spectral energy related to the zth packet coefficient at the Δf-bandwidth decomposition level, named as the zth packet energy, is computed as follows:

$$\mathcal{E}_{\Delta f}^z(k) = \sum_{n=k-N+1}^{k} \left[s_{\Delta f}^z(n) \right]^2, \qquad (4)$$

where $k \geq N$. Recursively, the zth packet energy can be obtained with a low computational burden as follows [31]:

$$\mathcal{E}_{\Delta f}^z(k) = \mathcal{E}_{\Delta f}^z(k-1) + \left[s_{\Delta f}^z(k) \right]^2 - \left[s_{\Delta f}^z(k-N) \right]^2, \quad (5)$$

which takes just two additions and one multiplication.

IV. THE PROPOSED HARMONIC MEASUREMENT METHOD

The novel harmonic measurement method, referred to as method W1, computes four harmonic energies related to the hth harmonic through packet energies at the $f/2$-bandwidth decomposition level. Two harmonic energies ($\mathcal{E}^{h+}$ and $\mathcal{E}^{h-}$) consider a long mother wavelet and a one-cycle sliding window. They are designed to estimate RMS harmonics in high precision during steady-state periods. These RMS values present a high time delay during transitions, while the remaining two harmonic energies ($\dot{\mathcal{E}}^{h+}$ and $\dot{\mathcal{E}}^{h-}$) consider a small mother wavelet and a half-cycle sliding window for estimating RMS harmonics with a reduced time delay during transient periods. Only one of these four harmonic energies is selected by employing two decision-making systems based on spectral energy variables. The first decision-making system selects harmonic energies to reduce the effect of interharmonics, whereas the second one selects harmonic energies to reduce the time delay.

A. Harmonic Estimation under Stationary PQ Disturbances

In real-time, the harmonic energy components $\mathcal{E}^{h+}$ and $\mathcal{E}^{h-}$ estimate the hth harmonic energy $\mathcal{E}^h$ under steady-state situations as follows:

$$\mathcal{E}^{h+}(k) = \mathcal{E}_{f/2}^{2h-1}(k)/\mathbb{E}_{f/2}^{2h-1}(hf) \qquad (6)$$

$$\mathcal{E}^{h-}(k) = \mathcal{E}_{f/2}^{2h}(k)/\mathbb{E}_{f/2}^{2h}(hf), \qquad (7)$$

where $h=\{1,2,3,...,h_{\max}\}$; the $f/2$-packet energies $\mathcal{E}_{f/2}^{2h-1}$ and $\mathcal{E}_{f/2}^{2h}$ are computed in (5) with $N = f_s/f$ (one-cycle RMS sliding window); $\mathcal{E}_{f/2}^{2h-1}$ and $\mathcal{E}_{f/2}^{2h}$ must be computed with long mother wavelets. This work uses the db(30) mother wavelet as further addressed in Section VII, where db(L) is the mother wavelet of the Daubechies family with L coefficients; the frequency-domain packet energies $\mathbb{E}_{f/2}^{2h-1}$ and $\mathbb{E}_{f/2}^{2h}$ are used as energy attenuation factors at the hth harmonic frequency hf and are obtained in a prior off-line analysis of the frequency response gain of the related packed energy.

B. Harmonic Estimation under Non-stationary Disturbances

In real time, the harmonic energy components $\dot{\mathcal{E}}^{h+}$ and $\dot{\mathcal{E}}^{h-}$ estimate the hth harmonic energy $\mathcal{E}^h$ under non-stationary PQ-disturbances as follows:

$$\dot{\mathcal{E}}^{h+}(k) = \dot{\mathcal{E}}_{f/2}^{2h-1}(k)/\mathbb{E}_{f/2}^{2h-1}(hf) \qquad (8)$$

or

$$\dot{\mathcal{E}}^{h-}(k) = \dot{\mathcal{E}}_{f/2}^{2h}(k)/\mathbb{E}_{f/2}^{2h}(hf), \qquad (9)$$

where $h=\{1,2,3,...,h_{\max}\}$; the $f/2$-packet energies $\dot{\mathcal{E}}_{f/2}^{2h-1}$ and $\dot{\mathcal{E}}_{f/2}^{2h}$ are computed using (5) with half-cycle RMS sliding window ($N = f_s/(2f)$) and the Haar filters, which are the lowest wavelet filters.

C. Detection of Transient Events

The proposed method detects transient events to support the decision-making systems when [29], [31], [56], [57]:

$$\mathcal{E}_{f_s/4}^1(k) > 2^2 E_{f_s/4}^1, \qquad (10)$$

$$\mathcal{E}_{f_s/4}^0(k) > 1.2^2 E_{f_s/4}^0, \qquad (11)$$

or

$$\mathcal{E}_{f_s/4}^0(k) < 0.8^2 E_{f_s/4}^0, \qquad (12)$$

is true, where $E_{f_s/4}^1$ and $E_{f_s/4}^0$ are average values of $\mathcal{E}_{f_s/4}^1$ and $\mathcal{E}_{f_s/4}^0$, respectively, during one cycle of the fundamental frequency.

The energy $\mathcal{E}_{f_s/4}^1$ is computed in the first decomposition level and is equal to the first-level wavelet coefficient energy of the SWT, which has been used for transient disturbance detection successfully [31], [56]. This energy is mainly affected by the highest frequency components of the signal, being scarcely influenced by subharmonics, low-frequency interharmonics, low-frequency harmonic distortions, and the fundamental component. This means $\mathcal{E}_{f_s/4}^1$ is sensitive to transients induced by non-stationary events such as faults and voltage sags, providing a fast detection [31], [56]. Based on statistical analysis in [31], [56], the number 2 in (10) is used to detect high-frequency transients in voltages or currents.

The energy $\mathcal{E}_{f_s/4}^0$ is also computed in the first decomposition level and is equal to the first-level scaling coefficient energy of the SWT. Contrary to $\mathcal{E}_{f_s/4}^1$, $\mathcal{E}_{f_s/4}^0$ is highly influenced by the fundamental component and low-order harmonics. Consequently, $\mathcal{E}_{f_s/4}^0$ has been used for detecting magnitude variations in the fundamental component in both voltages [29] and currents [57]. According to [29], voltage sags and swells are detected based on voltage thresholds of 0.9 and 1.1 p.u., with the energy thresholds of 0.9^2 and 1.1^2, respectively. However, this work uses the thresholds 0.8^2 and 1.2^2 to avoid the detection of slight voltage variations. Based on [57], current variations such as overcurrents are detected through thresholds in currents or squared thresholds in the energy analysis. Typical thresholds used in overcurrent protection could be used to detect current variations. However, for the sake of simplicity, 0.8 in (12) is used to detect undervoltages or undercurrents, whereas 1.2 in (11) is used to detect overvoltages or overcurrents.

Based on previous methods for detecting power system disturbances [29], [31], [56], [57], the detection of transient events using (10)-(12) will be able to detect non-stationary disturbances with voltage variations, current variations, and transients such as faults and voltage sags. These equations are independent and sensible to different signal frequency components, increasing the probability of correct detection. For instance, a voltage sag can be detected due to its transients using (10) or its voltage drop using (12).

D. Decision-making System to Reduce Interharmonic Effects

According to (6) and (7), $\mathcal{E}^{h+}$ and $\mathcal{E}^{h-}$ present a narrow frequency response of $f/2$, which reduce the affects of inter-harmonics. Furthermore, $\mathcal{E}^{h+}$ and $\mathcal{E}^{h-}$ redundantly estimate the hth harmonic energy $\mathcal{E}^h$ in different frequency spectra. Thus, the RMS calculation in (1) may use $\mathcal{E}^h=\mathcal{E}^{h+}$ or $\mathcal{E}^h=\mathcal{E}^{h-}$ in a way to be less affected by interharmonics as possible. $\mathcal{E}^{h+}$ and $\mathcal{E}^{h-}$ with $f/4$ is also possible if the signal presents strong interharmonic close to f.

$\Delta\mathcal{E}_{f/2}^{h+}$ is defined as the maximum value of $\mathcal{E}_{f/2}^{h+}$ minus the minimum value of $\mathcal{E}_{f/2}^{h+}$, considering only the last energies in one cycle of the fundamental frequency. In an analogue manner, $\Delta\mathcal{E}_{f/2}^{h-}$ is computed considering $\mathcal{E}_{f/2}^{h-}$. To reduce the interference of interharmonics, the decision-making system selects the hth harmonic energy with fewer oscillations according to the following simple algorithm:

- If $\Delta\mathcal{E}_{f/2}^{h+} \geq \Delta\mathcal{E}_{f/2}^{h-}$, then

$$\mathcal{E}^h(k) = \mathcal{E}^{h-}(k). \tag{13}$$

- Otherwise

$$\mathcal{E}^h(k) = \mathcal{E}^{h+}(k). \tag{14}$$

The values of $\Delta\mathcal{E}_{f/2}^{h+}$ and $\Delta\mathcal{E}_{f/2}^{h-}$ are updated once every cycle of the fundamental frequency.

E. Decision-Making System to Reduce the Time Delay During Transient Events

Another decision-making system handles the time delay in harmonic estimation under non-stationary PQ disturbances. If (10), (11), or (12) is true, the harmonics are estimated with a small mother wavelet and sliding window in order to reduce the time delay during transitions as follows:

- if (13) was previously selected:

$$\mathcal{E}^h(k) = \dot{\mathcal{E}}^{h-}(k); \tag{15}$$

- if (14) was previously selected:

$$\mathcal{E}^h(k) = \dot{\mathcal{E}}^{h+}(k). \tag{16}$$

Considering the db(30) mother wavelet and the decomposition process, the energy components defined in (6) and (7) converge to a new steady-state period in about 15 cycles from the transient event detection by using f_s=1600 Hz and f=50 Hz (or f_s=1920 Hz and f=60 Hz). Therefore, 15 cycles after transients, the proposed method considers back the previous selected energy defined in (13) or (14).

According to (13), (14), (15), and (16), only one of the energy variables $\mathcal{E}^{h+}$, $\mathcal{E}^{h-}$, $\dot{\mathcal{E}}^{h+}$, or $\dot{\mathcal{E}}^{h-}$ is selected to estimate the magnitude of the hth harmonic based on the existence of interharmonics and transient events.

V. EXISTING HARMONIC ESTIMATION METHODS

The performance of the proposed method is compared with two existing wavelet packet-based techniques, termed here as methods W2 and W3, the conventional DFT-based method with a one-cycle sliding window (DFT method), the modified cosine filter, the Mimic method, and the extended Kalman filter.

The method W2, proposed in [48], estimates RMS values of harmonics at an $f/2$-bandwidth decomposition level, and the packet energies are grouped to present a uniform f-bandwidth. The original method in [48] considered the DWPT based on the Vaidyanathan mother wavelet with 24 coefficients. Its window width with 10 cycles of the fundamental frequency is defined in the IEC Standard 61000-4-7. However, this paper uses the RT-SDWPT with a db(30) mother wavelet and a one-cycle sliding window to fairly compare with the proposed method W1.

The method W3, proposed in [41], estimates RMS values at a $2f$-bandwidth decomposition level by using the RT-SDWPT with Daubechies mother wavelets with 40 coefficients and a one-cycle sliding window of the fundamental frequency. Therefore, in this method only the Daubechies mother wavelet order was readjusted to 30 coefficients in order to fairly compare with the proposed method.

VI. ACTUAL DATA

The performance of the harmonic estimation methods was assessed with actual harmonic measurement data from: 1) commercially available household devices, acquired from PANDA Equipment Harmonic Database [58]; 2) an actual power transmission system with non-stationary PQ disturbances; and 3) a laboratory setup.

Fig. 1 shows two actual currents: i_X of a 50 Hz cathode-ray tube television (CRT TV) and i_Y of a 50 Hz liquid-crystal-display television (LCD TV), with i_X and i_Y sampled at f_s=1600 Hz. By using an offline frequency response analysis, Tables I and II summarise the magnitude and phase information of the main frequency components of these signals considering a normalization process which resulted in a signal with the fundamental RMS value of 1 p.u. Fig. 1 also shows realistic analytical signals $\bar{i}_X$ and $\bar{i}_Y$ with frequency components obtained from the actual signals i_X and i_Y (Tables I and II), respectively. $\bar{i}_X$ and $\bar{i}_Y$ present Gaussian white noise with SNR of 25 and 34 dB to suppress the disregarded interharmonics in i_X and i_Y, respectively. According to Fig. 1, the realistic analytical signals $\bar{i}_X$ and $\bar{i}_Y$ match quite well with the actual signals i_X and i_Y, respectively.

The currents i_X and $\bar{i}_X$ present several relevant odd harmonics, a second harmonic with low-magnitude, a DC component, and noise, whereas i_Y and $\bar{i}_Y$ present odd harmonics, even harmonics, a subharmonic, a few interharmonics, a DC component, and noise. The advantage of $\bar{i}_X$ and $\bar{i}_Y$ is that a specific frequency component, such as an interharmonic, can be adjusted to challenge harmonic estimation methods. In addition, $\bar{i}_X$ and $\bar{i}_Y$ can be reproduced in hardware to be evaluated in real time applications. Therefore, these realistic
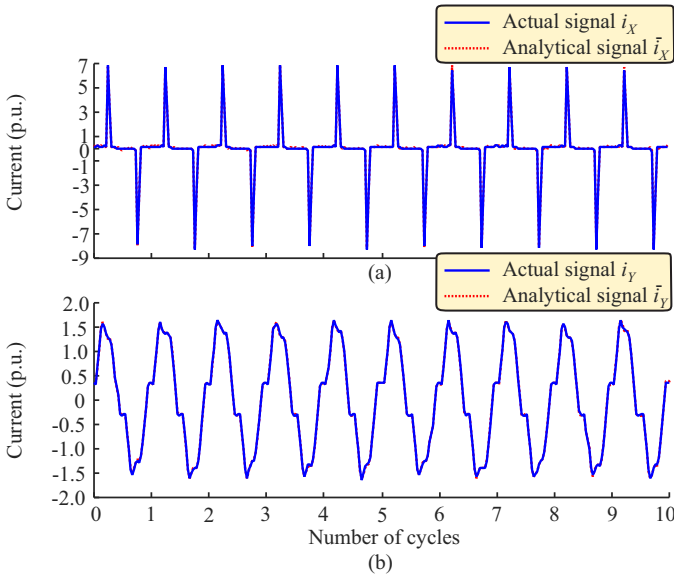
Fig. 1. Actual and analytical currents: a) i_X; b) i_Y.

analytical signals $\bar{i}_X$ and $\bar{i}_Y$, based on actual currents, can be used as benchmarks for evaluating harmonic estimation methods.

TABLE I
PARAMETERS OF THE ACTUAL CURRENT i_X.

RMS current (p.u.)		Phase angle (^{o})	
I_0	0.034595	-	-
I_1	1.000000	θ_1	0.504637
I_2	0.095613	θ_2	87.922766
I_3	0.936677	θ_3	169.963346
I_4	0.088738	θ_4	264.119948
I_5	0.860490	θ_5	-16.720857
I_6	0.081972	θ_6	80.620555
I_7	0.768640	θ_7	157.413175
I_8	0.072600	θ_8	259.654278
I_9	0.657754	θ_9	26.727809
I_{10}	0.062178	θ_{10}	78.464076
I_{11}	0.535460	θ_{11}	152.132314
I_{12}	0.053220	θ_{12}	260.317928
I_{13}	0.420331	θ_{13}	-23.449225
I_{14}	0.046890	θ_{14}	84.140133
I_{15}	0.346047	θ_{15}	170.051896

A commercial CINERGIA power converter, integrated into a smart grid laboratory [59], generated actual voltage signals with known harmonic distortions to assess the performance of RT-SDWPT-based methods with challenging situations. The voltage signals are a superposition of a fundamental frequency component (h=1) with a set of harmonics ($h \neq 1$) whose magnitudes were adjusted individually. The measurements were accomplished using a compact facility unit (manufactured by IMC) connecting the loads and energy sources to the smart grid laboratory. The facility unit contains security, communication, and measurement technology. The integrated voltage module sensors (HV-4U) obtained data with a measurement uncertainty less or equal to 0.05%.

The following actual voltages were generated and measured

TABLE II
PARAMETERS OF THE ACTUAL CURRENT i_Y.

RMS current (p.u.)		Phase angle (^{o})	
I_0	0.045600	-	-
$I_{sub,30}$	0.014040	$\theta_{sub,30}$	142.80
I_1	1.000000	θ_1	18.96
$I_{int,70}$	0.027280	$\theta_{int,70}$	179.40
I_2	0.003305	θ_2	201.70
$I_{int,130}$	0.001867	$\theta_{int,130}$	188.90
I_3	0.127000	θ_3	205.70
$I_{int,170}$	0.01813	$\theta_{int,170}$	-33.65
I_4	0.001104	θ_4	229.50
$I_{int,230}$	0.001304	$\theta_{int,230}$	231.20
I_5	0.153000	θ_5	205.80
$I_{int,270}$	0.001819	$\theta_{int,270}$	23.79
$I_{int,330}$	0.001126	$\theta_{int,330}$	-83.11
I_7	0.032460	θ_7	134.70
$I_{int,370}$	0.002140	$\theta_{int,370}$	11.40
$I_{int,430}$	0.001414	$\theta_{int,430}$	-30.01
I_9	0.016000	θ_9	242.50
$I_{int,470}$	0.001964	$\theta_{int,470}$	132.10
$I_{int,530}$	0.001463	$\theta_{int,530}$	6.07
I_{11}	0.007095	θ_{11}	10.40
$I_{int,570}$	0.001954	$\theta_{int,570}$	149.10
I_{13}	0.011620	θ_{13}	71.83
I_{15}	0.013840	θ_{15}	51.91

in the laboratory:

$$v_1(k) = 80\sqrt{2}\left[1.00\sin(1\omega k/f_s) + 0.90\sin(3\omega k/f_s)\right.$$
$$+ 0.80\sin(5\omega k/f_s + 120^\circ) + 0.70\sin(7\omega k/f_s)$$
$$\left. + 0.60\sin(9\omega k/f_s) + 0.50\sin(11\omega k/f_s)\right], \quad (17)$$

$$v_2(k) = 80\sqrt{2}\left[1.00\sin(1\omega k/f_s) + 0.95\sin(2\omega k/f_s)\right.$$
$$+ 0.90\sin(3\omega k/f_s) + 0.85\sin(4\omega k/f_s)$$
$$+ 0.80\sin(5\omega k/f_s) + 0.75\sin(6\omega k/f_s + 150^\circ)$$
$$\left. + 0.70\sin(7\omega k/f_s)\right], \quad (18)$$

where k={0,1,2,3,...}; the base voltage is 80 V RMS; f_s=10 kHz; ω=$2\pi f$, with f= {50, 51} Hz; v_1 presents only the fundamental frequency and odd harmonic components (h={1,3,5,7,9,11}), whereas v_2 presents both odd and even harmonic components (h={1,2,3,4,5,6,7}). Noise is inherently included in these actual signals mainly due to the signal generation and acquisition processes. The phase of each harmonic component was selected arbitrarily because in this study only RMS values are estimated.

Actual voltages with a subharmonic (v_3) and interharmonic (v_4) were also generated and measured as follows:

$$v_3(k) = v_2(k) + 0.2(80\sqrt{2})\sin(2\pi 30k/f_s), \quad (19)$$

$$v_4(k) = v_2(k) + 0.2(80\sqrt{2})\sin(2\pi 70k/f_s). \quad (20)$$

VII. PERFORMANCE ASSESSMENT

Actual signals with known RMS harmonic magnitudes are essential for validating harmonic estimation methods in challenge situations and for highlighting their advantages and disadvantages. In summary, the effects of sampling frequencies

(ideal and non-ideal values), frequency deviation, stationary and non-stationary PQ events, and the combination of different frequency components (odd harmonics, even harmonics, subharmonics, and interharmonics) were evaluated considering three wavelet-based methods and the method DFT. The performance results are summarized in Table III, with the proposed method presenting the best results. Detailed performance evaluation is addressed in the remainder of this section.

TABLE III
SUMMARY OF THE PERFORMANCE EVALUATION.

	Signal features					Performance of the methods			
Signal	f_s	f	odd	even	sub	int	W1	W2	W3	DFT
v_1	✓	50	✓				✓	✓	✓	✓
v_2	✓	50	✓	✓			✓	✓		✓
v_1	X	50	✓				✓	✓	✓	
v_2	X	50	✓	✓			✓	✓		
v_1	✓	51	✓				✓	✓	✓	
v_2	✓	51	✓	✓			✓	✓		
v_3	✓	50	✓	✓	✓		✓			
v_4	✓	50	✓	✓		✓	✓			

	Signal features	Performance of the methods			
Signal	non-stationary PQ disturbances	W1	W2	W3	DFT
X	✓	✓			✓

f_s with ✓ and X: ideal and non-ideal sampling frequency, respectively;
f=51 Hz: signal with frequency deviation; odd: odd harmonics;
even: even harmonics; sub: subharmonic; int: interharmonic;
signal with X: another signal beyond v_1, v_2, v_3, and v_4;
methods W1, W2, W3, and DFT with ✓: good results.

A. The Effects of Even Harmonics

The magnitude of the fundamental, second, third, and fifteenth harmonic components of the actual current i_X are I_1=1.000, I_2=0.096, I_3=0.937, and I_{15}=0.346 (Table I), respectively, where i_X does not present a relevant second harmonic magnitude. Nevertheless, the related analytical signal $\bar{i}_X$ presents the same harmonic content, with exception of the second harmonic, which was adjusted to a higher value of I_2=0.300 to highlight the effects of even harmonics. The SDWPT-based methods with db(30) mother wavelet and the DFT method instantaneously estimated RMS values of the fundamental, second, third, and fifteenth harmonic components of the actual current i_X, in ten cycles, as shown in Fig. 2. Table IV summarizes the average RMS values over 10 cycles in the currents i_X (Fig. 2) and $\bar{i}_X$.

TABLE IV
ESTIMATED RMS VALUES (AVERAGE OVER 10 CYCLES).

Signal	Order	Method				True value
		W1	W2	W3	DFT	
i_X	1st	1.00	1.00	1.00	1.00	1.00
	2nd	0.10	0.10	-	0.10	0.10
	3rd	0.94	0.94	0.94	0.94	0.94
	15th	0.35	0.35	0.35	0.35	0.35
$\bar{i}_X$	1st	1.00	1.00	1.04	1.00	1.00
	2nd	0.40	0.40	-	0.40	0.40
	3rd	0.94	0.94	0.98	0.94	0.94
	15th	0.35	0.35	0.35	0.35	0.35

Fig. 3 shows the frequency response of the methods W1, W2, and W3 with the mother wavelets db(30) and Haar
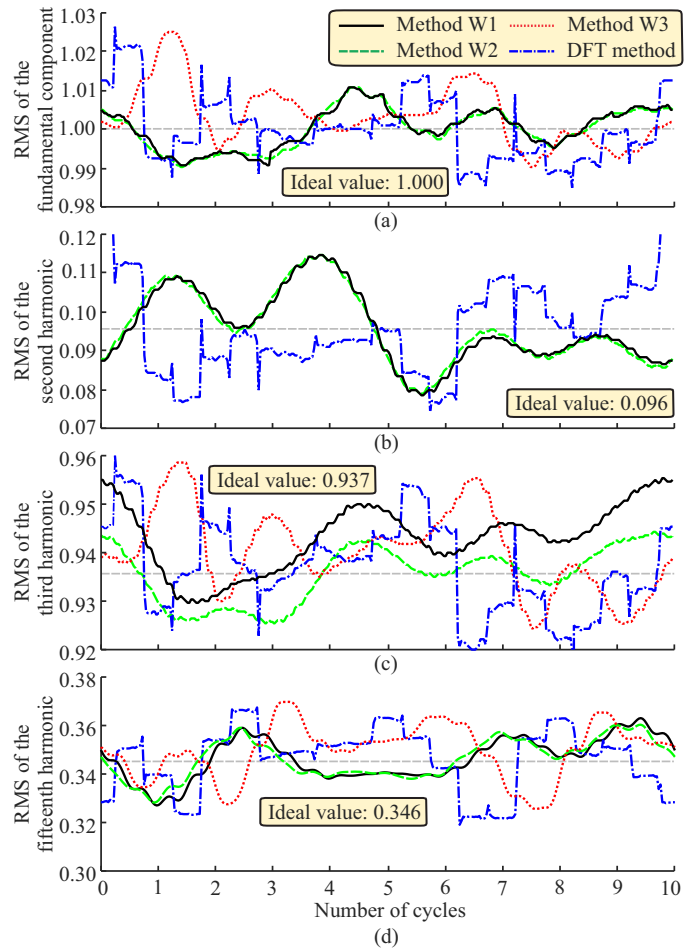

Fig. 2. Harmonic estimation of i_X: a) the fundamental component; b) the second harmonic component; c) the third harmonic component; d) the fifteenth harmonic component.

for signals sampled at f_s=1600 Hz and with fundamental frequency of f=50 Hz. The same analysis is true for f_s=1920 Hz and f=60 Hz. $\mathbb{E}_{\Delta f}^h$ is the frequency-domain packet energy gain of the related time-domain packet energy $\mathcal{E}_{\Delta f}^h$ obtained in an offline analysis with the Fourier transform. E_{cutoff}=1/2 is the ideal packet energy gain at the cutoff frequency.

The method W3 places odd harmonics at central frequencies with a minimum attenuation, whereas it places even harmonics at cutoff frequencies (Fig. 3(a)). Therefore, this method can only estimate odd harmonics accurately in situations where even harmonics and the DC component are disregarded. In Fig. 3(a), for instance, the second harmonic and the DC components highly affect the estimation of the fundamental component through $\mathcal{E}_{2f}^0$, whereas the second and fourth harmonics highly affect the estimation of the third harmonic component through $\mathcal{E}_{2f}^1$. According to Table IV, the method W3 only presented suitable and accurate RMS estimation of fundamental and third harmonic components in the signal i_X because the second harmonic presented a disregarded magnitude. Conversely, it presented deviations for the fundamental and third harmonic component estimation in the current $\bar{i}_X$ because the second harmonic was increased to 0.3 p.u. artificially. Thus, the method W3 could not estimate
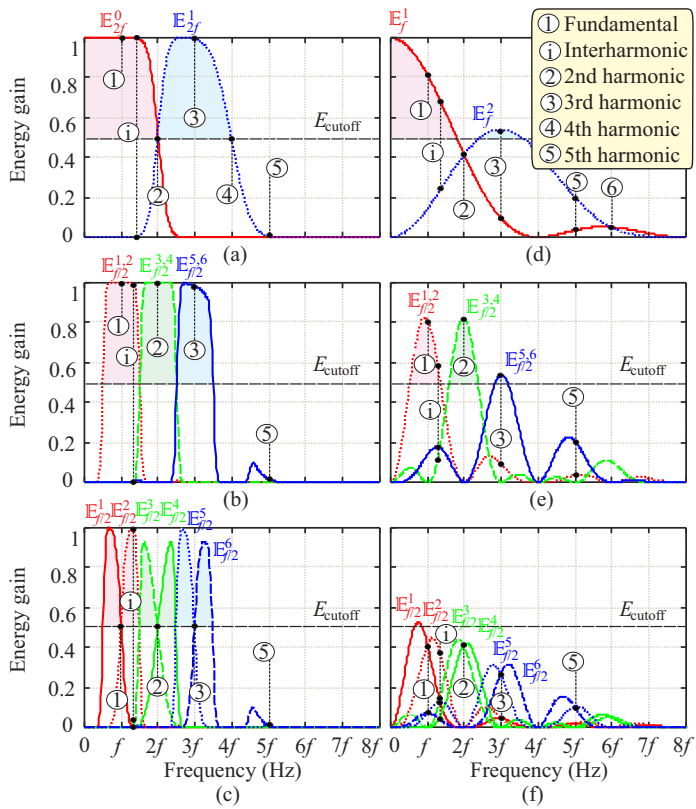
Fig. 3. Energy gain of some SDWPT packet-based methods: (a) W3 with db(30); (b) W2 with db(30); (c) W1 with db(30); (d) W3 with Haar; (e) W2 with Haar; (f) W1 with Haar.

even harmonics.

Only one harmonic mainly affects each energy variable in the methods W1 and W2. The method W2 places a specific harmonic in the central frequency of the energy variables (Fig. 3 (b)), whereas the method W1 places a specific harmonic in the cut-off frequency of the energy variables (Fig. 3 (c)). Therefore, the methods W1 and W2 overcome some limitations of the method W3 because they can estimate both odd and even components, such as the 1st (fundamental), 2nd, 3rd, 4th, and 5th, with scarce interference of other harmonics when they use a proper mother wavelet. Indeed, even harmonics did not affect the methods W1 and W2, and these methods presented an accurate performance for estimating both odd and even harmonics as presented in Table IV. The one-cycle DFT-based method presented similar results as the ones of methods W1 and W2.

B. Effects of the Mother Wavelet

The accuracy of the estimated RMS value depends on the frequency response of the wavelet filters. In general, the higher the wavelet filter order, the more accurate the estimate of the RMS value. Indeed, due to the best frequency response and lowest spectral leakage, the high-order wavelet filters in Figs. 3(a), (b), and (c) provide better harmonic estimation than the related low-order wavelet filters in Figs. 3(d), (e), and (f). The desired fundamental component and time-domain packet energy $\mathcal{E}_{2f}^0$ with db(30) in Fig. 3a) are also affected by

the DC and second harmonic components. With the Haar in Fig. 3(d), $\mathcal{E}_{2f}^0$ presents attenuation in the desired fundamental component, and is affected by the DC component and 2nd, 3rd, 5th, and 6th harmonic components.

According to Eqs. (17) and (18), v_1 presents no even harmonics, whereas v_2 presents strong even harmonics. Tables V and VI summarize the average RMS values over 10-cycles of the fundamental, second, and third harmonic components of v_1 and v_2, in per unit, obtained with the SDWPT-based methods with different mother wavelets. By using the mother wavelet db(30), the methods presented the desired precise results as in Table V. Only the method W3 was affected by the even harmonics in accordance with Section VII-A. Conversely, by using the Haar mother wavelet, all the wavelet-based methods presented errors as shown in Table VI. This is the main reason why the proposed and existing wavelet-based methods use high-order wavelet filters for RMS estimation of harmonics. The proposed method also uses the Haar wavelet during transient events as addressed in Section VII-H.

TABLE V
ESTIMATED RMS VALUES WITH db(30) (AVERAGE OVER 10 CYCLES).

Signal	Order	Method				True value
		W1	W2	W3	DFT	
v_1	1st	1.00	1.00	1.00	1.00	1.00
	2nd	0.00	0.00	-	0.00	0.00
	3rd	0.90	0.90	0.90	0.90	0.90
v_2	1st	1.00	1.00	1.20	1.00	1.00
	2nd	0.94	0.94	-	0.95	0.95
	3rd	0.90	0.90	1.26	0.90	0.90

TABLE VI
ESTIMATED RMS VALUES WITH HAAR (AVERAGE OVER 10 CYCLES).

Signal	Order	Method				True value
		W1	W2	W3	DFT	
v_1	1st	1.07	0.96	0.96	1.00	1.00
	2nd	0.00	0.00	-	0.00	0.00
	3rd	1.16	0.85	0.85	0.90	0.90
v_2	1st	1.06	0.96	1.14	1.00	1.00
	2nd	0.98	0.89	-	0.95	0.95
	3rd	1.14	0.84	1.17	0.90	0.90

C. Non-ideal Sampling Frequency

The sampling frequency f_s must be a multiple integer of $8f$ to place harmonic components in ideal frequency positions in the wavelet frequency response. Therefore, the signals with fundamental frequency of f=50 Hz were sampled at f_s=1600 Hz, which is an ideal sampling frequency for estimating RMS values of harmonics with order lower or equal to h_{max}=16, i.e., h={1,2,3,4,5,...,15,16}. Similarly, the signals with fundamental frequency of f=60 Hz were sampled at f_s=1920 Hz. As a consequence, the methods did not present errors associated to the selected sampling frequency in the previous results.

Depending on the application, the sampling frequency cannot be equal to the desired value, causing inaccuracy in

some methods. Therefore, instead of f_s=1600 Hz, v_1 and v_2 were now downsampled to f_s=1666.67 Hz to place harmonics in non-ideal positions in the frequency spectrum and verify the performance of the wavelet- and Fourier-based methods. Fig. 4 shows the instantaneous estimated RMS fundamental values of v_2 considering the db(30) mother wavelet. The SDWPT-based methods were not affected by a slight change in the ideal sampling frequency. Conversely, the instantaneous RMS estimation of the one-cycle DFT-based method presented considerable errors because the number of samples per cycle is no longer an integer value, which increases the spectral leakage.
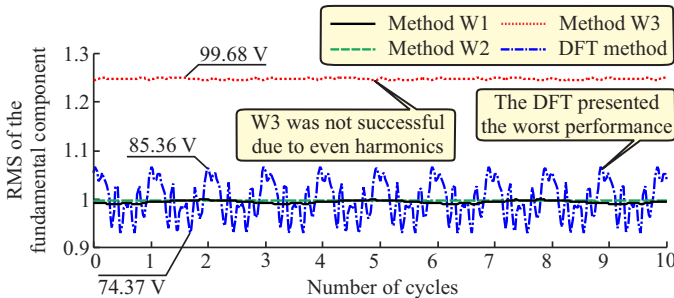
Fig. 4. Effects of non-ideal sampling frequency selection.

D. Frequency Deviation

Electrical power systems and power generators require operation at a constant frequency, and they do not tolerate operation with considerable frequency deviation. For instance, the IEEE Standard 1547 [60] presents requirements for the connection of distributed generation with the electric power system considering the frequency deviation limit from 58.5 to 61.2 Hz in a 60 Hz system. Furthermore, relays of frequency variation (ROCOF relays) typically operate for frequency deviations lower than 1.0 Hz.

The frequency deviation is also an issue for harmonic estimation methods. Therefore, the voltages v_1 and v_2 and related harmonics were also synthesized with the fundamental frequency of 51 Hz instead of 50 Hz, presenting a considerable frequency deviation. Fig. 5 shows the instantaneous estimated RMS values of the fundamental component of v_2, considering the db(30) mother wavelet. All the evaluated methods need a fundamental frequency estimation in the presence of frequency deviation to properly adjust the RMS window size and avoid spectral leakage errors. Since the frequency deviation in this analysis is known, and the development of a frequency estimation method is out of the scope of this paper, the one-cycle window in all methods was automatically adjusted for f=51 Hz and f_s=1600 Hz. Nevertheless, the harmonic estimation methods evaluated in this work can use any frequency estimation method.

The SDWPT-based methods were not affected by a fundamental frequency deviation of 1 Hz (Fig. 5). Conversely, even considering a window size adjustment, the DFT-based method provided instantaneous RMS estimation with considerable error because the number of samples per cycle is no longer an integer value, which increases the spectral leakage in this method.
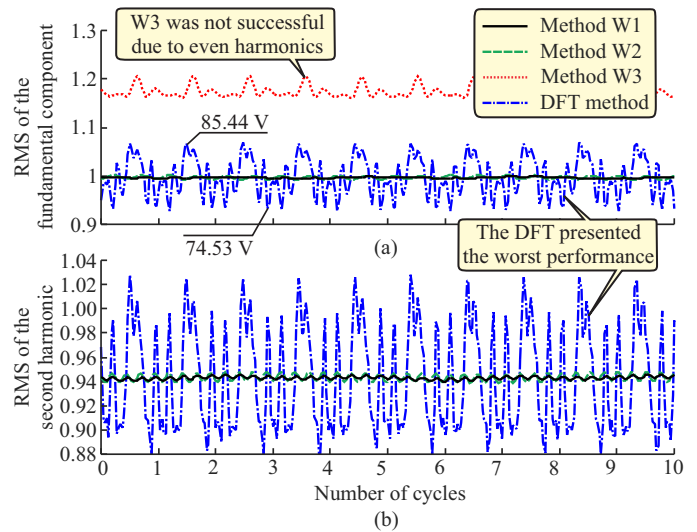

Fig. 5. Effects of frequency deviation in harmonic estimation: a) the fundamental component estimation; b) the second harmonic estimation.

E. Effects of Subharmonic and Interharmonic

Although the estimation of subharmonics and interharmonics is out of the scope of this study, these frequency components are major issues to wavelet- and Fourier-based harmonic estimation methods. Hence, the impact of their distortions in wavelet-based harmonic estimation methods must be evaluated.

The proposed method W1 is theoretically the least affected by subharmonics and interharmonics due to the narrow bandwidth of its packet energies and the redundancy in estimating a specific harmonic component. To prove this claim as far as the fundamental component estimation, Fig. 3 highlights the effects of an interharmonic ⓘ, located between the 1st and 2nd harmonic components (① and ②), in the wavelet-based methods. Fig. 6 depicts the effects of interharmonics in DFT-based methods. The main conclusions of this qualitative evaluation are as follows:

- Fig. 3(b): the method W2 centralizes each harmonic in a spectral bandwidth of grouped packet energies with a bandwidth of f Hz. Also, there is no redundancy to estimate harmonics, i.e., each harmonic is estimated with just one wavelet energy. Then, ⓘ strongly affects $\mathcal{E}_{f/2}^{1,2}$.
- Fig. 3(a): the method W3 presents the highest spectral bandwidth, being the most affected by interharmonics. ⓘ strongly affects $\mathcal{E}_{2f}^{0}$;
- Fig. 3(c): since the proposed method W1 places the wavelet cutoff frequency of two packet energies to each harmonic component, the fundamental component ① is placed at f in both $\mathcal{E}_{f/2}^{1}$ and $\mathcal{E}_{f/2}^{2}$ redundantly. In this case, ⓘ affects only $\mathcal{E}_{f/2}^{2}$. Then, $\mathcal{E}_{f/2}^{1}$ can estimate the fundamental component with scarce interference of ⓘ;
- Fig. 6(b): the one-cycle DFT-based method, usually taken as reference in most works, presents a high spectral bandwidth heavily affected by interharmonics.

Considering f_s=1600 Hz, Figs. 7 and 8 depict the instantaneous RMS values of the 1st and 2nd harmonic components of v_3 and v_4, which are actual voltages with subharmonic and
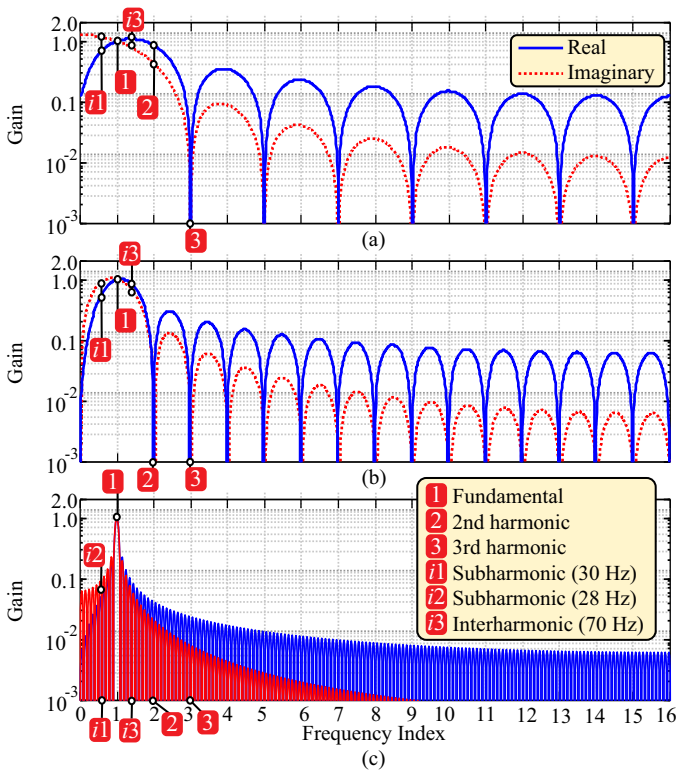
Fig. 6. Frequency response of DFT-based methods for estimating the fundamental component: a) half-cycle DFT; b) one-cycle DFT; c) ten-cycles DFT.
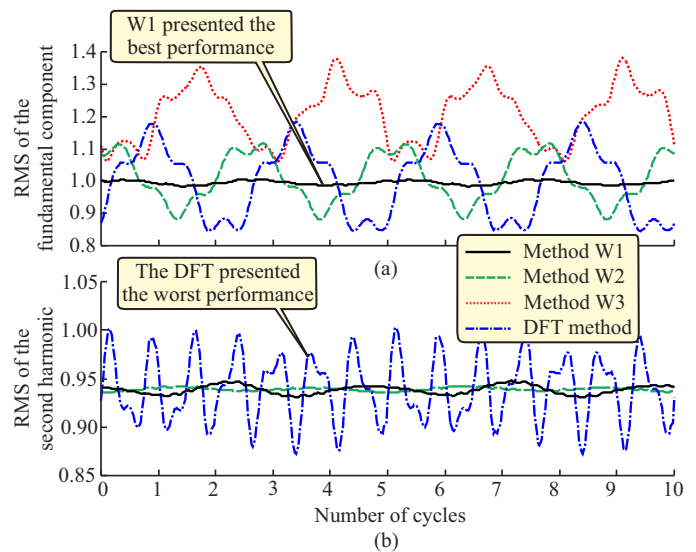

Fig. 7. Effects of subharmonics in harmonic estimation: a) the fundamental component estimation; b) the second harmonic estimation.
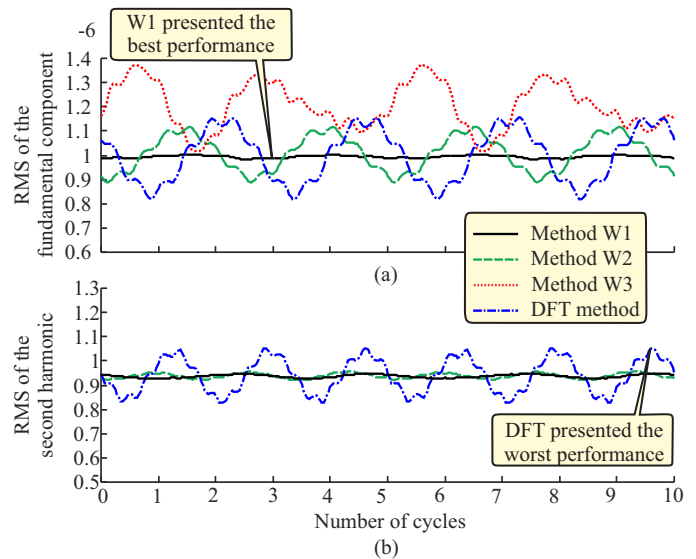

Fig. 8. Effects of interharmonics in harmonic estimation: a) the fundamental component estimation; b) the second harmonic estimation.

interharmonic, respectively, obtained with the SDWPT-based methods with the db(30) mother wavelet and the one-cycle DFT-based method. Only the proposed method W1 presented an accurate RMS estimation, whereas the methods W2, W3, and DFT were strongly affected by subharmonic and interharmonic components, presenting a considerable oscillation around the related average value. The RMS window of these methods were set to the size of the fundamental component. However, based on Fig. 6(b) and Figs. 3(a) and (b), the filtered signals contain attenuated interharmonics at 30 or 70 Hz in addition to the fundamental frequency component. Thus, presenting oscillations around the expected values.

In addition to the actual voltages v_3 and v_4, the actual current i_Y presents several interharmonics, with the most relevant non-harmonic components at frequencies of 30, 70, and 170 Hz according to Table II ($I_{sub,30}$=0.01, $I_{int,70}$=0.03, and $I_{int,170}$=0.02 p.u.). Therefore, the fundamental and second harmonic estimation is a major challenge for this signal due to the relevant subharmonic at 30 Hz and the relevant interharmonic at 70 Hz. The third harmonic estimation is also a challenge due to the relevant interharmonic at 170 Hz.

The actual signal i_Y (Fig. 1(b)) and its analytical signal version $\bar{i}_Y$ summarized in Table II are accurate versions of each other. An advantage of the analytical signal $\bar{i}_Y$ is that the interharmonic magnitude can be adjusted to a more challenging case. To additionally demonstrate the harmonic estimation challenges, the relevant non-harmonic components of i_Y were changed to $I_{sub,30}$=0.3, $I_{int,70}$=0.3, and $I_{int,170}$=0.3 p.u. in the analytical signal $\bar{i}_Y$. Fig. 9 depicts the 1st harmonic

estimations of the actual current i_Y, whereas Figs. 10, 11, and 12 depict the 1st, 2nd, and 3rd harmonic estimations of the actual-based analytical current $\bar{i}_Y$ shown in Fig. 1(b). The expected RMS values of the 1st, 2nd, and 3rd harmonics are 1.000, 0.003, and 0.127 p.u (Table II), respectively. Figs. 9 and 10 also present the performance of the DFT-based method with the modified cosine filter (ModCos) and Mimic method for estimating the RMS fundamental component. Figs. 9, 10, 11, and 12 also present the performance of the extended Kalman filter-based method described in [20].

According to Figs. 9 and 10, the proposed method W1, with an additional decomposition to narrow the frequency response of the energies, presented the most accurate RMS estimation of the 1st harmonic. The other methods provided considerable oscillations in the RMS estimation due to the interharmonics. For instance, the results of the full-cycle DFT
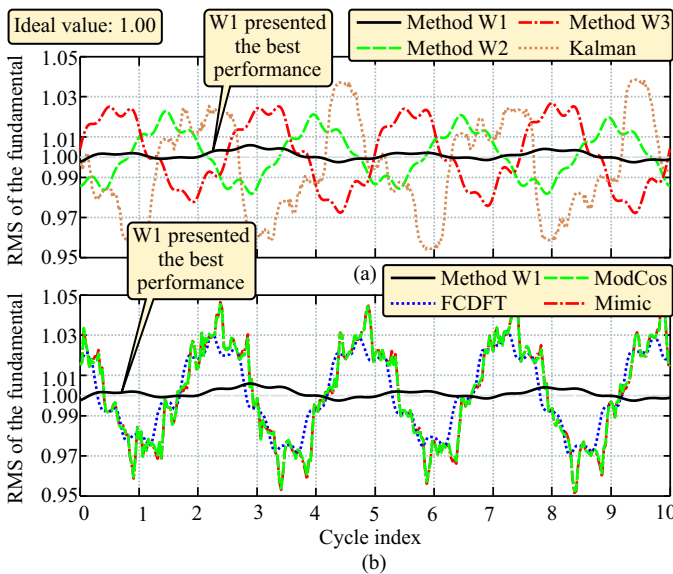
Fig. 9. The fundamental component estimation of the actual current i_Y with interharmonics: a) proposed, Kalman-based, and wavelet-based methods; b) proposed, Fourier-based, and other methods.
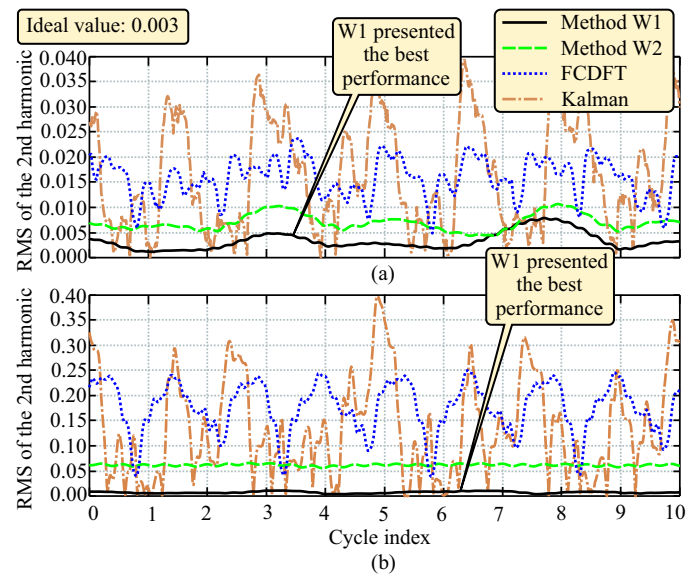

Fig. 11. The second harmonic estimation: a) actual current with interharmonics; b) analytical current with strong interharmonics.
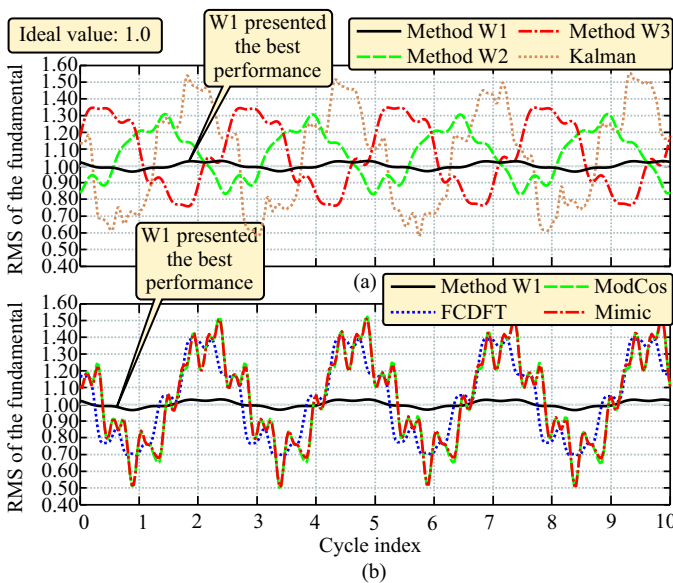

Fig. 10. The fundamental component estimation of the analytical current with strong interharmonics: a) proposed, Kalman-based, and wavelet-based methods; b) proposed, Fourier-based, and other methods.
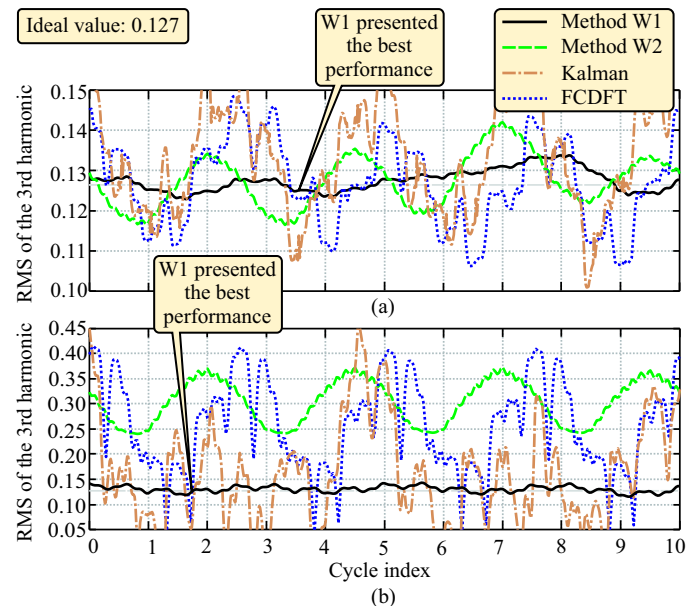

Fig. 12. The third harmonic estimation: a) actual current with interharmonics; b) analytical current with strong interharmonics.

(FCDFT) method oscillated from about 0.97 to 1.03 p.u. in Fig. 9 and from 0.7 to 1.4 p.u. in Fig. 10. The W2 and W3 methods performed slightly better than the FCDFT, whereas CosMod, Mimic, and extended Kalman filter were the most affected by interharmonics. Therefore, with the exception of the proposed method, all the evaluated methods presented impracticable results when the signal contains interharmonics.

The 2nd harmonic in i_Y and $\bar{i}_Y$ has a magnitude of 0.003305 p.u., which is difficult to be estimated in a signal with noise. In addition, i_Y presents an interharmonic with a magnitude of 0.027280 p.u. at the frequency of 70 Hz, which is a near interharmonic eight times greater than the 2nd harmonic. Thus, the estimation of the second harmonic of i_Y is

a challenge. To additionally challenge the harmonic estimators, $\bar{i}_Y$ has an interharmonic with a magnitude of 0.3 p.u. at the frequency of 70 Hz. According to Fig. 11, the proposed method W1 still presented an accurate RMS estimation in this tough case, whereas the other methods provided substantial errors with strong oscillations.

The estimation of the 3rd harmonic is also a challenge due to the near relevant interharmonic at the frequency of 170 Hz. According to Fig. 11, only the proposed method W1 presented accurate results, whereas the other methods provided substantial errors with strong oscillations.

F. Effects of Long RMS Window Size

Based on the IEC Standard 61000-4-7 [6], the DFT would present better RMS estimation results of harmonics in signals with interharmonics by replacing the one-cycle sliding window to a ten-cycle sliding window when f=50 Hz. The IEEE Standard 1459-2010 [7] defines the measurement of power quantities under sinusoidal and nonsinusoidal conditions based on RMS values of voltages and currents. Similarly, it recommends the DFT with a long window for estimating RMS values of harmonics in signals with interharmonics. According to the IEEE Standard 1459-2010, depending on the frequency of interharmonics, the DFT window size should be infinitely large to measure the RMS value or power correctly, which is impractical.
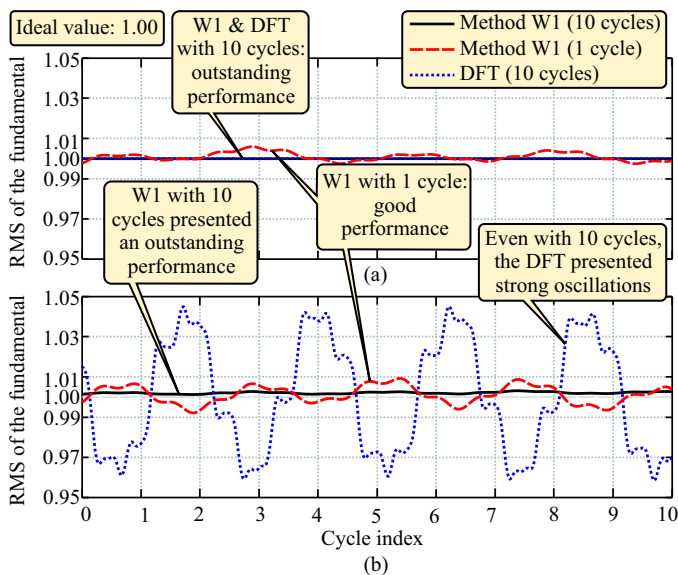

Fig. 13. The fundamental component estimation considering an: a) analytical current with strong interharmonics at 30, 70, and 170 Hz; b) analytical current with strong interharmonics at 28, 72, and 172 Hz.

Considering again the case shown in Fig. 10, where the actual-based synthetic signal presents strong interharmonics at frequencies of 30, 70, and 170 Hz ($I_{sub,30}$=0.3, $I_{int,70}$=0.3, and $I_{int,170}$=0.3 p.u.), the DFT with a one-cycle sliding window estimated the fundamental RMS component with a strong oscillation, whereas the proposed method with a one-cycle sliding window presented a good result with a minimum oscillation (Fig. 10(b)), as aforementioned. Using a ten-cycle window, the DFT presented an outstanding performance for this signal, as shown in Fig. 13(a). Indeed, except for the fundamental component at 50 Hz, all frequency components integer multiple of 5 Hz will be completely attenuated using a ten-cycle DFT (Fig. 6(c)). The proposed method is not limited to a basis of a one-cycle time window, and its window can be readjusted to attend to a specific standard or procedure. For instance, the proposed method with a ten-cycle window presented the same outstanding performance of the ten-cycle DFT in this signal.

Fig. 13(b) shows the performance of the DFT and W1 methods with a signal similar to that considered in Fig. 13(a). However, the strong interharmonic components are at frequencies of 28, 72, and 172 Hz ($I_{sub,28}$=0.3, $I_{int,72}$=0.3, and $I_{int,172}$=0.3 p.u.). In this case, the DFT presented a strong oscillation in the fundamental RMS component estimation even using a ten-cycle window. The DFT-based method would need the frequency information of all interharmonics to define an ideal window size to be used, which can be an impracticable window size depending on the interharmonic frequencies. Furthermore, the frequency estimation of interharmonics is a challenge in real-time applications. Conversely, the proposed method with a ten-cycle window still presented an exceptional performance for this case.

Based on the results shown in Fig. 13, a Fourier-based protective relay with typically one-cycle window size or any Fourier-based PMU or Fourier-based power quality monitoring devices with a window size of one or ten cycles would not perform well in some signals with interharmonics. Nevertheless, the proposed method presented good results with a one-cycle window and even better results with a ten-cycle window, demonstrating its potential as a possibility for protective relays, PMUs, or power quality monitoring devices.

G. Effects of Small RMS Window Size

Fig. 14 shows instantaneous estimated RMS values of the fundamental component for the signal with subharmonic v_3 considering one- and half-cycle algorithms (DFT and the proposed method W1). The half-cycle DFT presented the worst results, with oscillations reaching around 2.4 pu. These oscillations are because the half-cycle DFT, turned to estimate the fundamental component, is strongly affected by non-synchronous frequency components and even harmonics according to the DFT frequency response in Fig. 6(a).

For the SDWPT-based analysis, the RMS window is independent of the window to compute the packet coefficients, where the latter depends only on the mother wavelet. Therefore, the window size to compute the RMS values does not change the packet coefficients. As a consequence, the RMS values must be scarcely affected by the RMS window size. Indeed, according to Fig. 14, the proposed method W1 presented an accurate estimation of the RMS values with both half- and one-cycle RMS window lengths for v_3 with subharmonic.
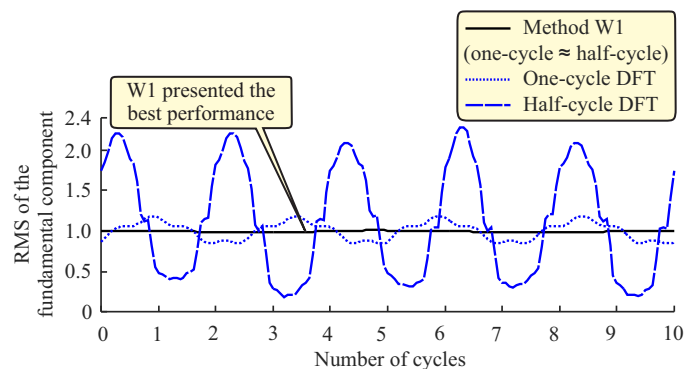

Fig. 14. Effects of RMS window length.

H. Effects of Non-stationary Power Quality Disturbances

The selection of low- and high-order wavelet filters is a trade-off. As addressed in Section VII-B, accurate harmonic component measurement requires mother wavelets with high-order filters due to their good frequency response, low spectral leakage, and low aliasing effects. Therefore, the proposed and existing methods use a mother wavelet with high-order filters. This is especially suitable for harmonic measurement in steady-state periods. However, a long wavelet filter can be an issue when transitions take place in the power system due to the great time delay. Unlike existing methods, the proposed method considers also the lowest wavelet filter (Haar filter) to overcome time delay issues during transient events.

The higher the wavelet filter length and the higher the wavelet decomposition level, the higher the time delay to estimate harmonics during transient events. The methods W1 and W2 need more decomposition levels than the method W3. For instance, the methods W1, W2, and W3 need five, five, and three decomposition levels to extract harmonic information by using f_s=1600 Hz and f=50 Hz (or f_s=1920 Hz and f=60 Hz), respectively. Therefore, considering long mother wavelets and various decomposition levels, these methods result in:

- High computational burden, which is no longer a problem to modern digital signal processors (DSPs);
- Considerable time delay for extracting information of non-stationary power quality disturbances, such as voltage sags, which can be an issue depending on the application. The proposed method W1, however, detects transient events (Section IV-C) to use a low-order wavelet filter during transient changes (Section IV-B), overcoming these problems.

Figs. 15 and 16 show the respective estimation of fundamental RMS values (RMS of the 1st harmonic) of an actual voltage with voltage sag and an actual current with an overcurrent. Both signals were measured in a 60 Hz power transmission system and normalized to present 1 p.u. in the steady-state period. The sampling frequency is f_s=1920 Hz. In Fig. 15, the 1st harmonic presents a hard decrease in magnitude for about three cycles, with a fast return to its original value. In Fig. 16, the magnitude of the 1st harmonic component increases slowly. Therefore, these scenarios consider non-stationary events with low- and high-rate of change of the fundamental component magnitude, a concern for harmonic estimation methods.

The RMS values in Figs. 15 and 16 were multiplied by $\sqrt{2}$ for the sake of illustrative simplicity. allowing for the RMS estimation can be compared to the waveform peaks. As expected, the method W2 presented a strong delay of about five cycles to estimate the fundamental component during the voltage sag (Fig. 15(a)) and the overcurrent (Fig. 16) because the filtering process considered both a long mother wavelet db(30) and five decomposition levels. Even using a reduced wavelet decomposition level, the method W3 presented a delay of about two cycles (Figs. 15(a) and 16), which is still long. The DFT-based method presented a delay of about one cycle (Figs. 15(a) and 16). If the size of the sliding window is changed from one to ten cycles to follow the IEC Standard
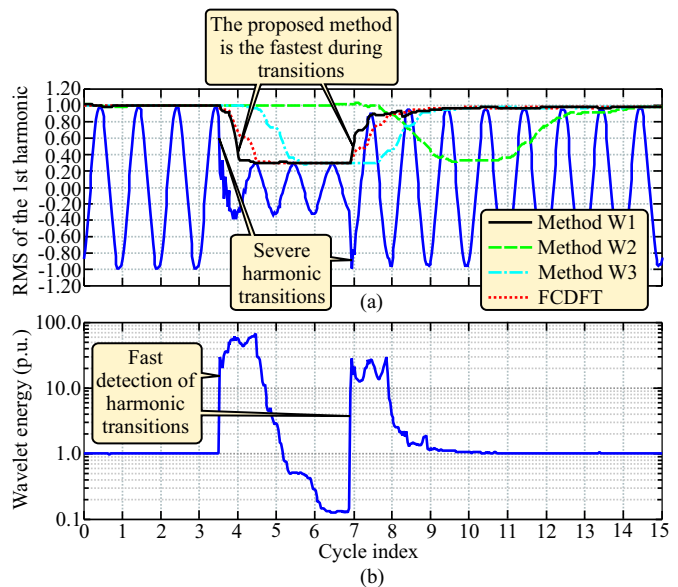

Fig. 15. Actual signal with a voltage sag: (a) RMS estimation of the $1st$ harmonic; (b) detection of non-stationary events.
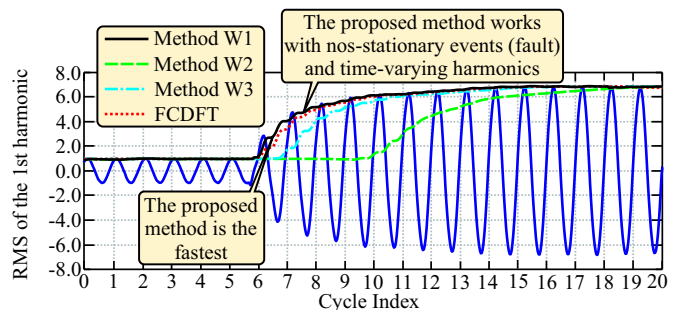

Fig. 16. The fundamental RMS estimation of an actual signal with overcurrent.

61000-4-7, it would present a delay of about ten cycles. The proposed method detected the beginning and end of the voltage sag and the beginning of the overcurrent with disregarded time delay (e.g., Fig. 15(b)). Thereafter, the mother wavelet was changed to the Haar wavelet, and the RMS window size was changed to half-cycle as proposed in Section IV-E. Therefore, the proposed method W1 presented the fastest RMS estimation of the fundamental component during the voltage sag (Fig. 15(a)) and overcurrent (Fig. 16) events. As a consequence, the proposed method presented accurate results during stationary and non-stationary PQ disturbances.
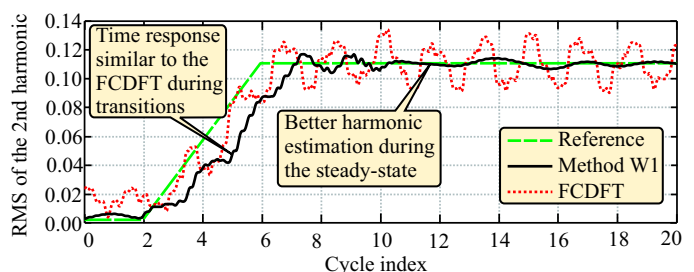
I. Effects of Time-varying Harmonics

Fig. 17. Effects of time-varying harmonics.

In addition to non-stationary events, the results obtained with actual voltage and current signals shown Figs. 15 and 16 respectively demonstrate that the proposed method also estimates RMS values of the time-varying fundamental component. However, the RMS estimation of harmonics with an order higher than one has the same principle as the RMS fundamental estimation. For instance, Fig. 17 depicts the RMS estimation of the 2nd harmonic of the actual-based analytical current $\bar{i}_Y$ shown in Fig. 1(b), where the RMS value increased in a ramping format from 0.003305 to 0.110000 A during four cycles of the fundamental. The RMS estimation of both the proposed and FCDFT-based methods converged to the expected value after the magnitude ramp variation with a similar time delay due to the filtering process. However, the proposed method was less affected by the interharmonics, presenting less RMS estimation variation.

J. Computational Burden

Considering a sampling frequency of f_s=1600 Hz, i.e., 32 samples per cycle of 50 Hz, the computation burden of the methods in a hardware implementation must be less than a sampling time of 625 μs to run in real-time.

The term $1/\sqrt{2}$ in (2) or (3) is a constant, which disappears when included in the filter coefficients for hardware implementation. Therefore, based on (2) or (3), each packet coefficient of the methods W1, W2, and W3 requires only addition and multiplication operations. These operations refer to Float point operations (FLOPs) in modern digital signal processors (DSPs). Therefore, each packet coefficient requires only 2L-1 FLOPs per decomposition level. In every sampling time, W1 and W2 require five decomposition levels and two packet coefficients per harmonic, whereas W3 requires four decomposition levels and one packet coefficient per harmonic. Therefore, for each RMS harmonic estimation, disregarding the memory management to store signals, W1 and W2 require 2*5(2L-1)=590 FLOPs per sampling time, whereas W3 requires 4(2L-1)=236 FLOPs per sampling time, to compute the packet coefficients. These methods also need to compute spectral energies, requiring just a few extra FLOPs in a recursive implementation according to [56].

Modern DSPs can perform millions of FLOPs per second (MFLOPS), such as the DSP TMS320C6748, which performs up to 2746 MFLOPS [61], i.e., 1,716,250 FLOPs per sampling time of 625 μs. Therefore, all the evaluated wavelet-based methods can run in real time using modern DSPs.

VIII. CONCLUSION

This paper proposed a comprehensive measurement method based on the stationary wavelet packet transform for the real-time RMS estimation of harmonic components. The performance evaluation considered representative and challenging actual signals from laboratory and field measurements to verify the effects of the mother wavelet, window length, sampling frequency, frequency deviation, subharmonic/interharmonic, harmonic fluctuation, and non-stationary disturbances. The proposed method outperformed the one-cycle discrete Fourier transform-based method and two existing wavelet packet

transform-based methods in terms of accuracy in all the evaluated cases.

As demonstrated by several studies, subharmonics and interharmonics present challenges for harmonic estimation methods. On the other hand, the proposed method accurately estimated the RMS values of odd and even harmonic components, even in situations with various interharmonics and subharmonics. The proposed method also presented promising harmonic estimation results in signals with an extreme frequency deviation of 1 Hz.

The performance assessment of harmonic estimation methods usually considers RMS values averaged in a given interval. However, the most suitable way to assess the performance of these methods is with instantaneous results, obtained sample-by-sample, as demonstrated in this study. Considering results in average values in an interval of ten cycles, the proposed method and most existing methods provided similar results near the expected RMS values. On the other hand, the proposed approach presented better results with flat RMS harmonic estimations, even in challenging cases. Existing evaluated methods presented considerable oscillations around the expected results, which may limit the usage of harmonic estimation methods in real-time practical applications, such as in harmonic measurement and mitigation devices.

Harmonic estimation during non-stationary power quality events, such as voltage sags, is also a challenge in applications that need instantaneous harmonic estimation. The existing methods provided impracticable long-time delay for harmonic estimation in an actual voltage sag, whereas the proposed method was the fastest because it efficiently detects transient events and temporarily uses a low-order filter.

With the sample-by-sample harmonic magnitude estimation, flexibility to change the time window size to attend specific standards, and good results even in signals with strong multiple interharmonics, the proposed method presents a potential to be used in power quality monitoring devices after the inclusion of other parameter estimation, such as phase angle estimation.

IX. FURTHER WORK

Fig. 18 depicts the actual-based synthetic current with inter-harmonics $\bar{i}_Y$ and its real fundamental component i_{h1}. $\bar{i}_Y$ is based on the actual signal i_Y (Table II), and the only changing is the presence of strong inter-harmonics at frequencies of 30, 70, and 170 Hz ($I_{sub,30}$=0.3, $I_{int,70}$=0.3, and $I_{int,170}$=0.3 p.u.). The proposed method has demonstrated outstanding performance in harmonic magnitude estimation considering actual signals with challenging situations. For instance, even with strong interharmonics in the signal $\bar{i}_Y$, the proposed method presented a flat RMS estimation of the 1st, 2nd, and 3rd harmonics in Figs. 10, 11(b), and 12(b), respectively.

According to Section IV, the proposed method uses the spectral energy of a specific wavelet signal to estimate the magnitude of each harmonic. i_{h1-W1} in Fig. 18(a) is the selected wavelet signal to compute the spectral energy and estimate the magnitude of the 1st harmonic of $\bar{i}_Y$ shown in Fig. 10. Even with strong interharmonics surrounding this harmonic component, i_{h1-W1} represents a sinusoidal signal
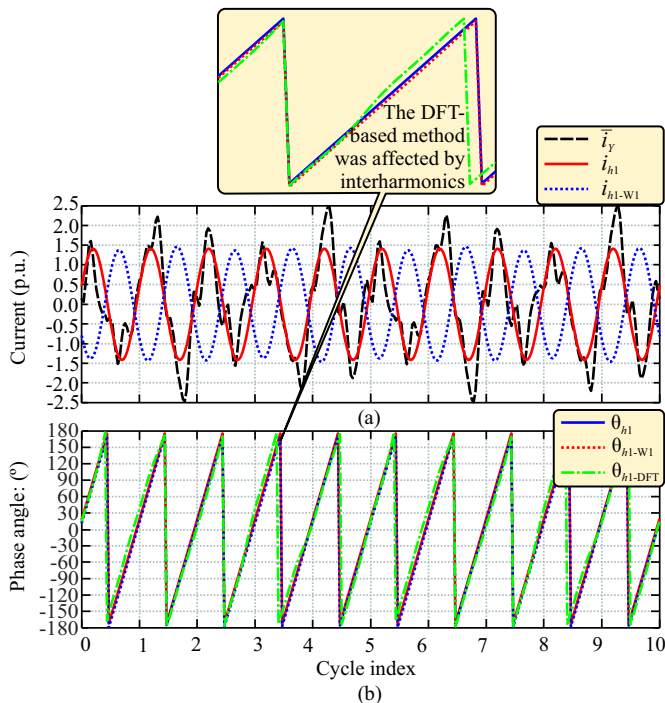
Fig. 18. Preliminary phase estimation: (a) currents; (b) pahse angles.

with the fundamental frequency and with strong attenuation of the other frequency components. Therefore, the magnitude estimation of the 1st harmonic with the proposed method presented an accurate performance in Fig. 10.

Comparing the wavelet signal i_{h1-W1} obtained with the proposed method and the actual fundamental component i_{h1} of the signal $\bar{i}_Y$ in Fig. 18(a), i_{h1-W1} presents a time delay. However, the time delay is a known parameter obtained from the frequency response of the wavelet filters. Therefore, the phase angle of the 1st harmonic can be easily obtained with any method by using i_{h1-W1} instead of the original signal with interharmonics $\bar{i}_Y$ because i_{h1-W1} must only present the desired frequency component. For instance, considering a signal with only the fundamental component, such as i_{h1-W1}, one of the simplest way to estimate the phase angle is to apply the inverse tangent function to i_{h1-W1} and i_{h1-W1} with a phase displacement of 90 degrees. The result is the phase angle estimation θ_{h1-W1} as shown in Fig. 18(b), which fits the reference value θ_{h1}. This idea can be extended to the other harmonics.

Discrete versions of the wavelet transform, which usually use real mother wavelet, present mathematical limitations for estimating phase angle [62], [63]. Therefore, the discrete versions of the wavelet transform have been claimed to be unsuitable for harmonic phasor measurements. Nevertheless, based on this preliminary result, discrete wavelet transforms with real mother wavelet can estimate harmonic phase angle.

Fig. 18(b) also depicts the phase angle estimation of the 1st harmonic using the FCDFT (θ_{h1-DFT}). In addition to strong errors in the magnitude estimation in Fig. 10(b), θ_{h1-DFT} also presented errors in Fig. 18(b) because the DFT is highly affected by interharmonics, whereas the proposed method performed better in Fig. 18(b) with an elementary phase angle

estimation.

The proposed wavelet-based method estimates harmonic phasor instantaneous magnitude. However, a rigorous harmonic phasor estimation is essential in power quality monitoring, protection, and control of power systems. Therefore, further work should consider the extension of the proposed method to include an estimate of harmonic phasor phase, frequency, and rate of change of frequency to be effective in signals with interharmonics.

REFERENCES

[1] S. K. Jain, P. Jain, and S. N. Singh, "A fast harmonic phasor measurement method for smart grid applications," *IEEE Transactions on Smart Grid*, vol. 8, no. 1, pp. 493–502, 2017.

[2] K. Duda, T. P. Zieliński, A. Bień, and S. H. Barczentewicz, "Harmonic phasor estimation with flat-top fir filter," *IEEE Trans. Instrum. Meas.*, vol. 69, no. 5, pp. 2039–2047, 2020.

[3] J. Sun, E. Aboutanios, D. B. Smith, and J. E. Fletcher, "Robust frequency, phase, and amplitude estimation in power systems considering harmonics," *IEEE Trans. Power Del*, vol. 35, no. 3, pp. 1158–1168, 2020.

[4] L. Chen, W. Zhao, X. Xie, D. Zhao, and S. Huang, "Harmonic phasor estimation based on frequency-domain sampling theorem," *IEEE Trans. Instrum. Meas.*, vol. 70, pp. 1–10, 2021.

[5] Z. Zecevic and B. Krstajic, "Dynamic harmonic phasor estimation by adaptive taylor-based bandpass filter," *IEEE Transactions on Instrumentation and Measurement*, vol. 70, pp. 1–9, 2021.

[6] "IEC 61000-4-7. electromagnetic compatibility EMC - part 4-7: Testing and measurement techniques-general guide on harmonics and interharmonics measurement and instrumentation, for power supply systems and equipment connected thereto," *International Electrotechnical Commission*, 2002.

[7] "IEEE standard definitions for the measurement of electric power quantities under sinusoidal, nonsinusoidal, balanced, or unbalanced conditions," *IEEE Std 1459-2010 (Revision of IEEE Std 1459-2000)*, pp. 1–50, Mar. 2010.

[8] K. M. Silva and F. A. O. Nascimento, "Modified dft-based phasor estimation algorithms for numerical relaying applications," *IEEE Transactions on Power Delivery*, vol. 33, no. 3, pp. 1165–1173, 2018.

[9] L. Ibarra, D. Guillen, J. Avilés, P. Ponce, and A. Molina, "A fourier-based phasor estimator with a modified moving average filter and its application in distribution networks," *IEEE Transactions on Industrial Informatics*, vol. 18, no. 1, pp. 698–706, 2022.

[10] J. K. Hwang, C. K. Song, and M. G. Jeong, "Dft-based phasor estimation for removal of the effect of multiple dc components," *IEEE Transactions on Power Delivery*, vol. 33, no. 6, pp. 2901–2909, 2018.

[11] J. K. Hwang and C. S. Lee, "Fault current phasor estimation below one cycle using fourier analysis of decaying dc component," *IEEE Transactions on Power Delivery*, vol. 37, no. 5, pp. 3657–3668, 2022.

[12] G. Benmouyal, "Removal of dc-offset in current waveforms using digital mimic filtering," *IEEE Trans. Power Del.*, vol. 10, no. 2, pp. 621–630, 1995.

[13] D. G. Hart, D. Novosel, and R. A. Smith, "Modified cosine filters," *U.S. Patent 6,154,687*, Nov. 2000.

[14] K. W. Min and S. Santoso, "Dc offset removal algorithm for improving location estimates of momentary faults," *IEEE Transactions on Smart Grid*, vol. 9, no. 6, pp. 5503–5511, 2018.

[15] L. Lai, W. Chan, C. Tse, and A. So, "Real-time frequency and harmonic evaluation using artificial neural networks," *IEEE Transactions on Power Delivery*, vol. 14, no. 1, pp. 52–59, 1999.

[16] H. C. Lin, "Intelligent neural network-based fast power system harmonic detection," *IEEE Transactions on Industrial Electronics*, vol. 54, no. 1, pp. 43–52, 2007.

[17] S. Katyara, L. Staszewski, and Z. Leonowicz, "Signal parameter estimation and classification using mixed supervised and unsupervised machine learning approaches," *IEEE Access*, vol. 8, pp. 92 754–92 764, 2020.

[18] I. Sadinezhad and V. G. Agelidis, "Real-time power system phasors and harmonics estimation using a new decoupled recursive-least-squares technique for dsp implementation," *IEEE Transactions on Industrial Electronics*, vol. 60, no. 6, pp. 2295–2308, 2013.

[19] U. Subudhi, H. K. Sahoo, and S. K. Mishra, "Harmonics and decaying dc estimation using volterra lms/f algorithm," *IEEE Transactions on Industry Applications*, vol. 54, no. 2, pp. 1108–1118, 2018.

[20] M. Uner, "Frequency, amplitude, and phase tracking of nonsinusoidal signal in noise with extended kalman filter," Ph.D. dissertation, Naval Postgraduate School, 1991.

[21] S. K. Singh, N. Sinha, A. K. Goswami, and N. Sinha, "Several variants of kalman filter algorithm for power system harmonic estimation," *International Journal of Electrical Power Energy Systems*, vol. 78, pp. 793–800, 2016.

[22] X. Nie, "Detection of grid voltage fundamental and harmonic components using kalman filter based on dynamic tracking model," *IEEE Transactions on Industrial Electronics*, vol. 67, no. 2, pp. 1191–1200, 2020.

[23] W. Zhou, O. Ardakanian, H.-T. Zhang, and Y. Yuan, "Bayesian learning-based harmonic state estimation in distribution systems with smart meter and dpmu data," *IEEE Transactions on Smart Grid*, vol. 11, no. 1, pp. 832–845, 2020.

[24] P. Garanayak, R. T. Naayagi, and G. Panda, "A high-speed master-slave adaline for accurate power system harmonic and inter-harmonic estimation," *IEEE Access*, vol. 8, pp. 51 918–51 932, 2020.

[25] C. Altintasi, "Sine cosine algorithm approaches for directly estimation of power system harmonics amp; interharmonics parameters," *IEEE Access*, vol. 9, pp. 73 169–73 181, 2021.

[26] Y. Terriche, A. Laib, A. Lashab, C.-L. Su, J. M. Guerrero, and J. C. Vasquez, "A frequency independent technique to estimate harmonics and interharmonics in shipboard microgrids," *IEEE Transactions on Smart Grid*, vol. 13, no. 2, pp. 888–899, 2022.

[27] M. Heydarzadeh, M. Zafarani, M. Nourani, and B. Akin, "A wavelet-based fault diagnosis approach for permanent magnet synchronous motors," *IEEE Trans. Energy Conv.*, vol. 34, no. 2, pp. 761–772, 2019.

[28] A. Pigazo, M. Liserre, R. A. Mastromauro, V. M. Moreno, and A. Dell'Aquila, "Wavelet-based islanding detection in grid-connected pv systems," *IEEE Trans. Ind. Electron.*, vol. 56, no. 11, pp. 4445–4455, Nov. 2009.

[29] F. B. Costa and J. Driesen, "Assessment of voltage sag indices based on scaling and wavelet coefficient energy analysis," *IEEE Trans. Power Del.*, vol. 28, no. 1, pp. 336–346, Jan. 2013.

[30] K. L. V. Iyer, X. Lu, Y. Usama, V. Ramakrishnan, and N. C. Kar, "A twofold daubechies-wavelet-based module for fault detection and voltage regulation in seigs for distributed wind power generation," *IEEE Trans. Ind. Electron.*, vol. 60, no. 4, pp. 1638–1651, Apr. 2013.

[31] F. B. Costa, "Fault-induced transient detection based on real-time analysis of the wavelet coefficient energy," *IEEE Trans. Power Del.*, vol. 29, no. 1, pp. 140–153, Feb. 2014.

[32] ——, "Boundary wavelet coefficients for real-time detection of transients induced by faults and power-quality disturbances," *IEEE Trans. Power Del.*, vol. 29, no. 6, pp. 2674–2687, Dec. 2014.

[33] M. de Apráiz, J. Barros, and R. I. Diego, "A real-time method for time-frequency detection of transient disturbances in voltage supply systems," *Elect. Power Syst. Res.*, vol. 108, pp. 103 – 112, 2014.

[34] M. B. Latran and A. Teke, "A novel wavelet transform based voltage sag/swell detection algorithm," *Int. J. Electr. Power and Energy Syst.*, vol. 71, pp. 131 – 139, 2015.

[35] S. Khokhar, A. A. M. Zin, A. P. Memon, and A. S. Mokhtar, "A new optimal feature selection algorithm for classification of power quality disturbances using discrete wavelet transform and probabilistic neural network," *Measurement*, vol. 95, pp. 246 – 259, Oct. 2017.

[36] M.-F. Guo, N.-C. Yang, and L.-X. You, "Wavelet-transform based early detection method for short-circuit faults in power distribution networks," *Int. J. Electr. Power and Energy Syst.*, vol. 99, pp. 706 – 721, Feb. 2018.

[37] J. Barros and R. I. Diego, "Analysis of harmonics in power systems using the wavelet-packet transform," *IEEE Trans. Instrum. Meas.*, vol. 57, no. 1, pp. 63–69, Jan. 2008.

[38] E. Y. Hamid, R. Mardiana, and Z.-I. Kawasaki, "Method for rms and power measurements based on the wavelet packet transform," *IEE Proc. Sci., Meas. and Technol.*, vol. 149, no. 2, pp. 60–66, Mar. 2002.

[39] I. Urbina-Salas, J. R. Razo-Hernandez, D. Granados-Lieberman, M. Valtierra-Rodriguez, and J. E. Torres-Fernandez, "Instantaneous power quality indices based on single-sideband modulation and wavelet packet-hilbert transform," *IEEE Trans. Instrum. Meas.*, vol. 66, no. 5, pp. 1021–1031, May. 2017.

[40] E. Y. Hamid and Z.-I. Kawasaki, "Instrument for the quality analysis of power systems based on the wavelet packet transform," *IEEE Power Eng. Rev.*, vol. 22, no. 3, pp. 52–54, Mar. 2002.

[41] V. K. Tiwari, A. C. Umarikar, and T. Jain, "Fast amplitude estimation of harmonics using undecimated wavelet packet transform and its hardware implementation," *IEEE Trans. Instrum. Meas.*, vol. 67, no. 1, pp. 65–77, Jan. 2018.

[42] W.-K. Yoon and M. J. Devaney, "Power measurement using the wavelet transform," *IEEE Trans. Instrum. Meas.*, vol. 47, no. 5, pp. 1205–1210, Oct. 1998.

[43] ——, "Reactive power measurement using the wavelet transform," *IEEE Trans. Instrum. Meas.*, vol. 49, no. 2, pp. 246–252, Apr. 2000.

[44] W. G. Morsi and M. E. El-Hawary, "Reformulating power components definitions contained in the IEEE standard 1459-2000 using discrete wavelet transform," *IEEE Trans. Power Del.*, vol. 22, no. 3, pp. 1910–1916, July 2007.

[45] ——, "Reformulating three-phase power components definitions contained in the IEEE standard 1459-2000 using discrete wavelet transform," *IEEE Trans. Power Del.*, vol. 22, no. 3, pp. 1917–1925, July 2007.

[46] A. H. Ghaemi, H. A. Abyaneh, and K. Mazlumi, "Harmonc indices assessment by wavelet transform," *Int. J. Electr. Power Energy Syst.*, vol. 33, no. 8, pp. 1399 – 1409, 2011.

[47] C. A. Naik and P. Kundu, "Power quality index based on discrete wavelet transform," *Int. J. Electr. Power Energy Syst.*, vol. 53, pp. 994 – 1002, 2013.

[48] J. Barros and R. I. Diego, "A new method for measurement of harmonic groups in power systems using wavelet analysis in the IEC standard framework," *Elect. Power Syst. Res.*, vol. 76, no. 4, pp. 200–208, Sep. 2006.

[49] F. Vatansever and A. Ozdemir, "Power parameters calculations based on wavelet packet transform," *Int. J. Electr. Power and Energy Syst.*, vol. 31, no. 10, pp. 596 – 603, 2009.

[50] W. G. Morsi and M. El-Hawary, "Novel power quality indices based on wavelet packet transform for non-stationary sinusoidal and non-sinusoidal disturbances," *Elect. Power Syst. Res.,*, vol. 80, no. 7, pp. 753–759, 2010.

[51] R. I. Diego and J. Barros, "Global method for time - frequency analysis of harmonic distortion in power systems using the wavelet packet transform," *Elect. Power Syst. Res.*, vol. 79, no. 8, pp. 1226 – 1239, Apr. 2009.

[52] ——, "Subharmonic measurement using dft and wavelet-packet transform in an iec extended framework," *Measurement*, vol. 43, no. 10, pp. 1603–1608, Sep. 2010.

[53] J. Modarresi and R.-A. Hooshmand, "A new combined method for rms calculation based on wavelet packet and hilbert transform," *Turkish J. Electr. Eng. Comput. Sci.*, vol. 24, pp. 3178–3197, Jan. 2016.

[54] S. Mallat, *A wavelet tour of signal processing*. Academic Press, 2008.

[55] D. K. Alves, F. B. Costa, R. L. A. Ribeiro, C. M. S. Neto, and T. O. A. Rocha, "Real-time power measurement using the maximal overlap discrete wavelet-packet transform," *IEEE Trans. Ind. Electron.*, vol. 64, no. 4, pp. 3177–3187, Apr. 2017.

[56] R. P. Medeiros, F. B. Costa, and K. M. Silva, "Power transformer differential protection using the boundary discrete wavelet transform," *IEEE Trans. Power Del.*, vol. 31, no. 5, pp. 2083–2095, Oct. 2016.

[57] F. B. Costa, A. Monti, and S. Paiva, "Overcurrent protection in distribution systems with distributed generation based on the real-time boundary wavelet transform," *IEEE Trans. Power Del.*, vol. PP, no. 99, pp. 1–1, 2015.

[58] "Panda equipment harmonic database. Dresden University of Technology. available online: www.panda.et.tu-dresden.de."

[59] C. Wiezorek, A. Parisio, T. Kyntaja, J. Elo, M. Gronau, K. H. Johannson, and K. Strunz, "Multi-location virtual smart grid laboratory with testbed for analysis of secure communication and remote co-simulation: concept and application to integration of berlin, stockholm, helsinki," *IET Gener. Transm. Distrib*, vol. 11, no. 12, pp. 3134–3143, 2017.

[60] "IEEE standard for interconnection and interoperability of distributed energy resources with associated electric power systems interfaces," *IEEE Std 1547-2018 (Revision of IEEE Std 1547-2003)*, 2018.

[61] "Tms320c6748 fixed- and floating-point dsp datasheet, 2009, texas instruments."

[62] F. Fernandes, R. van Spaendonck, and C. Burrus, "A new framework for complex wavelet transforms," *IEEE Transactions on Signal Processing*, vol. 51, no. 7, pp. 1825–1837, 2003.

[63] M. Sumner, A. Abusorrah, D. Thomas, and P. Zanchetta, "Real time parameter estimation for power quality control and intelligent protection of grid-connected power electronic converters," *IEEE Transactions on Smart Grid*, vol. 5, no. 4, pp. 1602–1607, 2014.